

Research Articles



Polymer Chemistry

How to cite: Angew. Chem. Int. Ed. 2024, 63, e202402747 doi.org/10.1002/anie.202402747

Copper Nanodrugs by Atom Transfer Radical Polymerization

Peng Chen⁺, Ziyan Song⁺, Xuxia Yao, Weibin Wang, Lisong Teng, Krzysztof Matyjaszewski,* and Weipu Zhu*

Abstract: In this study, some copper catalysts used for atom transfer radical polymerization (ATRP) were explored as efficient anti-tumor agents. The aqueous solution of copper-containing nanoparticles with uniform spheric morphology was in situ prepared through a copper-catalyzed activator generated by electron transfer (AGET) ATRP in water. Nanoparticles were then directly injected into tumor-bearing mice for antitumor chemotherapy. The copper nanodrugs had prolonged blood circulation time and enhanced accumulation at tumor sites, thus showing potent antitumor activity. This work provides a novel strategy for precise and large-scale preparation of copper nanodrugs with high antitumor activity.

[*] P. Chen, T. Song, W. Zhu

MOE Key Laboratory of Macromolecular Synthesis and Functionalization

Department of Polymer Science and Engineering

Zhejiang University

Hangzhou 310027, China

E-mail: zhuwp@zju.edu.cn

K. Matyjaszewski

Department of Chemistry

Carnegie Mellon University

Pittsburgh, Pennsylvania 15213, United States

E-mail: km3b@andrew.cmu.edu

X. Yao

School of Materials Science and Engineering

Zhejiang University

Hangzhou 310027, China

W. Wang, L. Teng

The First Affiliated Hospital

Department of Surgical Oncology

Zhejiang University School of Medicine

Hangzhou 310003, China

W. Zhı

Shanxi-Zheda Institute of Advanced Materials and Chemical

Engineering

Taiyuan 030000, China

W. Zhı

Key Laboratory of Adsorption and Separation Materials & Technologies of Zhejiang Province

Zhejiang University

Hangzhou 310027, China

[+] These authors contributed equally to this work.

Introduction

Platinum complexes represented by cisplatin are most widely used metal complexes as chemotherapeutic drug,[1] but the side effects and resistances greatly limited their clinical applications, which have prompted researchers to develop substitution strategies based on other metals.^[2] As an essential trace element in human body, copper is involved in a variety of biological pathways.[3] In recent years, numerous studies have shown that some copper complexes can exert cytotoxicity on a variety of tumor cells by targeting DNA, [4] inducing reactive oxygen species (ROS), [5] inhibiting topoisomerases^[6] or inhibiting the proteasome.^[7] A recent work pointed out that some copper complexes induce cell death through a mechanism of cuproptosis (direct binding of copper to lipoylated components of the tricarboxylic acid cycle).[8] Therefore, copper complexes have the potential to be developed as novel anticancer drugs.

Conventional chemotherapy drugs indiscriminately cause damage to normal human tissues due to the lack of selectivity of small-molecule drugs toward tumor tissue, [9] leading to severe toxic side effects and various complications while killing tumor cells, which bring great pain to patients.[10] Nanodrug is an important option to reduce the toxic side effects of anticancer drugs, improving the selectivity of drugs to tumor sites by enhanced permeability and retention (EPR)[11] or active targeting,[12] which is an important direction of research in the field of anticancer drugs. [13] Despite years of research, only a few nanodrugs have been approved for clinical use.^[14] The preparation process of typical nanodrugs involves the synthesis of carriers, and the loading of drugs to carriers to form nanoparticles.^[15] Each step requires the separation and purification of the products. On the milligram level at a laboratory, it is relatively easy to precisely regulate each step and achieve sophisticated preparation of nanodrugs with complex structures and functions. However, for nanodrugs to be translated into clinical applications, it is also necessary to be able to establish a manufacturing process that meets good manufacturing practice (GMP), and has the ability to achieve batch production. Under the conditions of large-scale preparation, multi-step processes cause a serious challenge to the precise preparation of nanodrugs, which becomes one of the major obstacles to the clinical translation of nanodrugs. [13b]

Copper complexes have been widely used in the field of catalysis owing to their excellent catalytic activities. Among the chemical reactions catalyzed by copper complexes, atom transfer radical polymerization (ATRP) is extremely attrac-



tive, which has been extensively studied since its invention in 1995. ATRP is a versatile strategy for the preparation of polymers with narrow molecular weight distribution, block copolymers and nanomaterials owing to the controlled/living polymerization nature.^[16] The complexation constants of copper complexes vary under different ATRP catalytic [tetradentate (cyclic-bridged), tetradentate (branched), tetradentate (cyclic), tridentate, and bidentate ligands],[17] while studies have shown that when copper ions and ligands are weakly bonding, the copper complexes will have strong tendency to release copper ions and thus show high cytotoxicity for cancer cells.^[18] Therefore, it is possible to precisely design copper nanodrug directly through ATRP using a copper catalyst with a low complexation constant.

In this work, we proposed a strategy to simplify the synthesis of copper nanodrugs, as shown in Figure 1. Copper complexes with tridentate ligands with both ATRP catalytic capacity and anticancer activity were prepared and used as catalysts for the miniemulsion activator generated by electron transfer (AGET) ATRP. The copper catalysts with anticancer activity were in situ incorporated in the miniemulsion colloids, to form an aqueous dispersion of

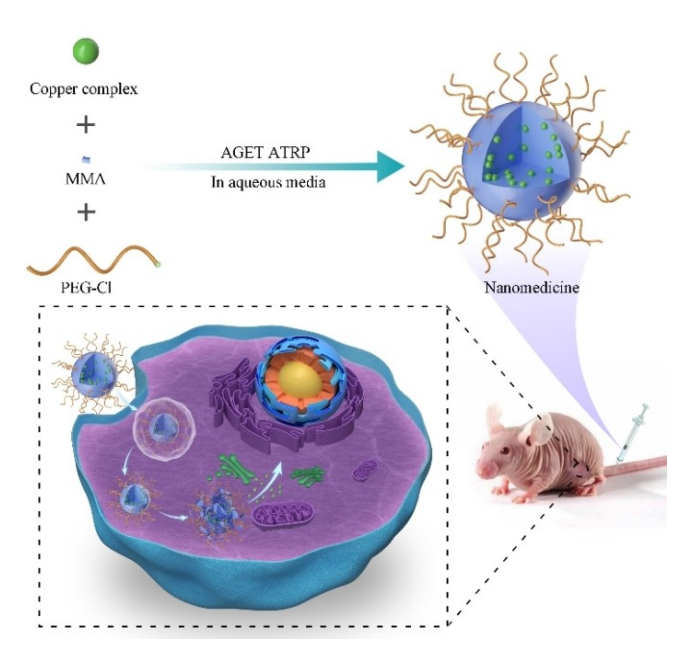


Figure 1. Preparation of copper-containing nanodrug.

copper nanodrug in a one-step reaction. They could be directly used for anticancer chemotherapy through intravenous injection. This method largely simplifies the preparation steps, and reduces the complexity of the system, and makes it more effective than that of conventional polymeric nanodrugs. This method provides an efficient approach for the batch production of nanodrugs for some antitumor copper complexes that may be clinically applied in the future and is expected to facilitate their clinical translation. [21]

Results and Discussion

Synthesis and Antitumor Activity of ATRP Catalysts

A series of copper complexes were synthesized from CuCl₂ with various ligands, such as 2,2'-bipyridine (bpy), 4,4'-di(5nonyl)-2,2'-bipyridine (dNbpy), 1,1,4,7,7-pentamethyldiethylenetriamine (PMDETA), 1,1,4,7,10,10-hexamethvltriethylenetetramine (HMTETA), tris[2-(dimethylamino)ethyl|amine (Me₆TREN), bis (2-pyridylmethyl) octadecylamine (BPMODA), with proton nuclear magnetic resonance (¹H NMR) shown in Figure S1, Bis [2-(4-methoxy-3,5-dimethyl)pyridylmethyl] octadecylamine (BMMO-DA) (¹H NMR shown in Figure S2), were characterized by FT-IR (Figure S3-S9) and elemental analysis (Table S1). Figure S3-S9 shows the increase of wavenumbers for the inplane aromatic ring stretches and C-N stretches for ligands after coordination by copper, which was consistent with the electronic effect caused by the coordination of nitrogen to copper. Table S1 shows that the results from elemental analysis are in agreement with the theoretical values, indicating the accurate composition of the obtained copper complexes.

MDA-MB-231 (Human breast cancer cell line), HuH-7 (Human hepatoma cell line), HT-1080 (Human fibrosarcoma cell line) and HCT-116 (Human colon cancer cell line) were used to evaluate the anticancer activity of the copper complexes by cell counting kit-8 (CCK-8) assay. The cytotoxicity of the clinical appliable metal-based anticancer agent cisplatin was also studied as a comparison. As shown in Table 1, Cu(PMDETA)Cl₂ and Cu(HMTETA)Cl₂ showed lower anticancer efficacy compared with other copper complexes. This result can be attributed to their high water solubility and strong binding strength between copper

Table 1: Cytotoxicity of copper complexes, and cisplatin to different tumor cells. Data are represented by mean \pm SD, n=3.

Entry	Compounds	IC ₅₀ (μM)					
		MDA-MB-231	HuH-7	HT-1080	HCT-116		
1	Cisplatin	123.00 ± 0.08	90.19±6.06	154.83 ± 22.21	84.43 ± 8.74		
2	$Cu(bpy)_2Cl_2$	84.27 ± 7.87	124.29 ± 10.44	36.00 ± 3.90	17.28 ± 0.39		
3	Cu(PMDETA)Cl ₂	181.13 ± 2.27	242.22 ± 13.73	> 300	280.58 ± 13.66		
4	Cu(HMTETA)Cl ₂	> 300	> 300	> 300	> 300		
5	Cu (Me ₆ TREN) Cl ₂	> 300	> 300	> 300	> 300		
6	Cu(dNbpy) ₂ Cl ₂	20.46 ± 2.00	19.24 ± 0.63	$\textbf{6.23} \pm \textbf{0.05}$	12.38 ± 0.10		
7	Cu(BPMODA)Cl ₂	1.76 ± 0.19	1.78 ± 0.32	3.02 ± 0.03	1.51 ± 0.08		
8	Cu(BMMODA)Cl ₂	1.88 ± 0.41	1.46 ± 0.07	2.69 ± 0.49	2.20 ± 0.25		

ion and ligand resulting from their tetradentate structure, [16i,22] hindering the transportation and release of copper ion into the cancer cell. [18a-c] Due to the strong hydrophobicity brought by the alkyl group, Cu-(BPMODA)Cl₂ and Cu(BMMODA)Cl₂ exhibited highest cytotoxicity against all four kinds of tumor cells according to the evaluation criteria in the literature, [18d] with IC₅₀s less than 4 µM, and Cu(dNbpy)₂Cl₂ showed moderate cytotoxicity against the four kinds tumor cells with IC50s less than 25 µM. At the same time, cisplatin showed relatively weak antitumor activity, with $IC_{50}s$ all above 80 μM , which were 20-fold higher than those receiving Cu(BPMODA)Cl₂ or Cu(BMMODA)Cl₂. These results indicated that part of copper complexes possessed antitumor activity higher than cisplatin, which generally showed good antitumor potential for biomedical applications. Based on the above results, Cu(dNbpy)₂Cl₂, Cu(BPMODA)Cl₂ and Cu(BMMODA)Cl₂ were finally used as catalysts for the preparation of antitumor copper nanodrugs.

Preparation of Copper Nanodrugs by Miniemulsion AGET ATRP

Poly(ethylene glycol) methyl ether 2-chloroisobutyrate (PEG–Cl, M_n =5,000) (¹H NMR spectrum shown in Figure S10) was used as both macroinitiator and stabilizer because of the nontoxic and protein resistance properties of poly(ethylene glycol) (PEG),^[23] to prepare nanoparticles through miniemulsion AGET ATRP of methyl methacrylate (MMA) as monomer and copper complexes as catalysts in aqueous medium as shown in Table 2. For Cu(dNbpy)₂Cl₂, at the stage of material mixing and miniemulsion preparation, the freshly prepared miniemulsion converted rapidly to the emulsion with the precipitation of catalyst out from miniemulsion particles. This result may derive from the mismatch between the hydrophobicity of the Cu(dNbpy)₂Cl₂ and the emulsifying ability of the stabilizer PEG–Cl chosen for this reaction system, resulting in the poor control of the

polymerization. For Cu(BMMODA)Cl2, with the ratio of monomer to initiator decreasing from 600:1 to 100:1, the monomer conversion increased from 94.7% to 99.7%, indicating the high conversion of MMA. The glass transition temperature (T_g) of poly(methyl methacrylate) (PMMA) homopolymer should be around 110°C, [24] and MMA could not be completely polymerized below 70°C. The solid sample of Entry 12 in Table 1 was obtained by lyophilization, which was characterized by differential scanning calorimetry (DSC) as shown in Figure S11. Meanwhile, the same sample was purified by dissolving in tetrahydrofuran (THF) and precipitation in methanol, to form a pure block copolymer for DSC measurement. The purified block copolymer has a glass transition temperature of 86.3 °C for PMMA block. However, the Tg of PMMA block in the nanoparticles decreased to 53.5 °C, which may be attributed to the plasticization by Cu(BMMODA)Cl₂. [25]

The loading efficiency was defined as the percentage of the copper complexes encapsulated in the nanoparticles, which reflected the encapsulation efficiency of the antitumor agent. All the copper that remained in the final product was in the form of copper (II), since any copper (I) was spontaneously oxidized to copper (II) after polymerization under an air atmosphere. The loading efficiencies of Cu-(BPMODA)Cl₂ and Cu(BMMODA)Cl₂ were above 90 % (Entry 5 to 12, Table 2). In addition, the change of molecular weight followed the feed change and conversion, while the molecular weight distribution remained narrow, as expected for ATRP. As confirmed by the ¹H NMR (Figure S12) spectroscopy, the ratios of MMA units to PEG in the copolymer corresponded to the feed and conversion. The particle size decreased with the shortening of the hydrophobic PMMA segment, while the particle size polydispersity index (PDI) remained narrow. Similar results were obtained using Cu(BPMODA)Cl₂ as a catalyst. The products of entry 8 and entry 12 in Table 2 prepared at high monomer conversion, high copper loading efficiency, and suitable particle size, were selected for further anticancer

Table 2: Preparation of nanodrugs via AGET ATRP using different copper catalysts. [a]

Entry	Catalysts	[M]/[I]	Conv ^[b]	Load efficiency of Cu complex ^[c]	Solid content ^[d]	Particle size ^[e]			Molecular weight ^[f]
	•	,	(%)	(%)	(%)	Diameter(nm)	PDI	$M_{\rm n}(\times 10^4)$	$M_{\rm w}/M_{\rm n}$
1	Cu(dNbpy) ₂ Cl ₂	600:1	13.3	10.2	6.7	227.7	0.424	1.21	1.43
2	Cu(dNbpy) ₂ Cl ₂	300:1	16.2	14.9	6.1	216.1	0.388	0.93	1.59
3	Cu(dNbpy) ₂ Cl ₂	200:1	20.4	12.1	6.0	176.6	0.257	0.91	1.42
4	Cu(dNbpy) ₂ Cl ₂	100:1	26.4	8.3	5.4	160.8	0.218	0.72	1.57
5	Cu(BPMODA)Cl ₂	600:1	92.7	95.3	31.5	115.9	0.105	6.41	1.25
6	Cu(BPMODA)Cl ₂	300:1	96.4	95.6	21.0	98.6	0.104	3.29	1.12
7	Cu(BPMODA)Cl ₂	200:1	98.8	93.6	16.4	92.7	0.091	2.80	1.32
8 ^[g]	Cu(BPMODA)Cl ₂	100:1	99.7	91.2	10.6	84.9	0.114	1.80	1.13
9	Cu(BMMODA)Cl ₂	600:1	94.7	94.7	32.1	97.5	0.072	6.04	1.24
10	Cu(BMMODA)Cl ₂	300:1	96.5	93.5	21.0	81.8	0.071	3.32	1.30
11	Cu(BMMODA)Cl ₂	200:1	99.4	94.0	16.5	76.9	0.071	2.37	1.14
12	Cu(BMMODA)Cl ₂	100:1	99.7	90.7	10.6	72.6	0.091	1.68	1.17

[a] [l]/[CuL]/[A]=4:4:1 (molar ratio), M: MMA, I: PEG—Cl, CuL: complex, A: ascorbic acid. [Hex]=3 wt% [M], hex: hexadecane. 70 °C, 6 hours. [b] Measured by gas chromatograph (GC). [c] The proportion of copper complexes distributed inside the nanocarrier, measured by inductively coupled plasma-optical emission spectrometer (ICP-OES). [d] The weight fraction of the nanodrugs in the final latex product. [e] Measured by dynamic light scattering (DLS). [f] Measured by gel permeation chromatography (GPC). [g] Solid content was 10.6%, and other entries increase the amount of monomer on this basis.

5213773, 2024, 20, Downloaded from https://onlinelibtary.wiley.com/doi/10.1002/anie.020402747 by Carnegie Mellon University, Wiley Online Library on [1/4/03/2025]. See the Terms and Conditions (https://onlinelibrary.wiley.com/terms-and-conditions) on Wiley Online Library for rules of use; OA articles are governed by the applicable Creative Commons License and Conditions (https://onlinelibrary.wiley.com/terms-and-conditions) on Wiley Online Library for rules of use; OA articles are governed by the applicable Creative Commons License and Conditions (https://onlinelibrary.wiley.com/terms-and-conditions) on Wiley Online Library for rules of use; OA articles are governed by the applicable Creative Commons License and Conditions (https://onlinelibrary.wiley.com/terms-and-conditions) on Wiley Online Library for rules of use; OA articles are governed by the applicable Creative Commons License and Conditions (https://onlinelibrary.wiley.com/terms-and-conditions) on Wiley Online Library for rules of use; OA articles are governed by the applicable Creative Commons License and Conditions (https://onlinelibrary.wiley.com/terms-and-conditions) on Wiley Online Library for rules of use; OA articles are governed by the applicable Creative Commons License and Conditions (https://onlinelibrary.wiley.com/terms-and-conditions) on Wiley Online Library for rules of use and the use of use and use an

investigation, donating as BP-nano and BM-nano, respectively.

The particle size and morphology of BP-nano and BM-nano were analyzed by transmission electron microscope (TEM), as shown in Figure 2a and 2b, indicating the uniform spherical morphologies with particle sizes of 76.0 nm and 74.5 nm for both nanodrugs respectively (calculated by Nano Measurer 1.2.5). This agreed with the DLS results obtained for miniemulsion polymerization^[26] (Figure 2c and 2d). The particle size and morphology measured by DLS and TEM both demonstrated the uniformity of BP-nano and

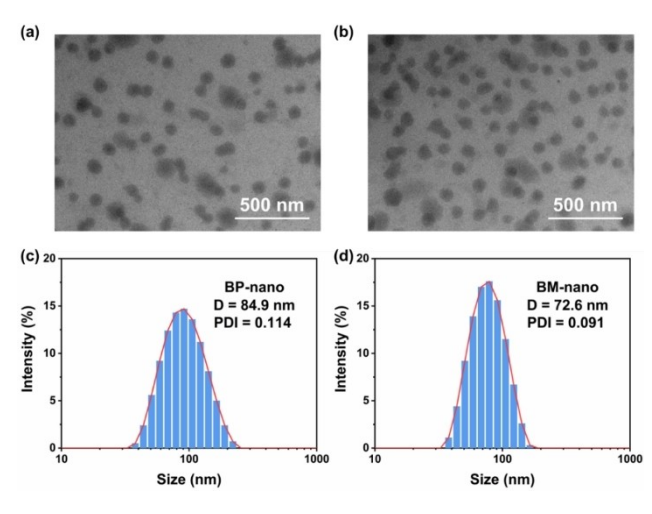


Figure 2. TEM images of the BP-nano (a) and BM-nano (b). DLS curves of the BP-nano (c) and BM-nano (d).

BM-nano nanoparticles, beneficial for the applications as a nanodrug.^[27]

Stability of Copper Nanodrugs

As shown in Figure 3a and 3b, the particle size and PDI of BP-nano and BM-nano did not change significantly even after 28 days, indicating good stability of the nano structures of BP-nano and BM-nano. Meanwhile, the copper loading efficiency of BM-nano remained constant during 28 days without any precipitation observed. However, the copper loading efficiency of BP-nano decreased significantly with the blue precipitate of copper complex at the flask bottom (Figure 3c). The methoxy and two methyl groups in BMMODA made Cu(BMMODA)Cl₂ incorporated more stably in the hydrophobic core of nanoparticles than Cu-(BPMODA)Cl₂. Based on the above results, BM-nano was chosen as the candidate for further comprehensive study.

The stability of BM-nano under simulated physiological and blood conditions was investigated with phosphate buffered saline (PBS) and fetal bovine serum (FBS). 1 mg/mL of nanodrug in PBS solution or PBS solution containing 10 % FBS were prepared by adding nanodrug to the corresponding solution, mixed thoroughly, and stored in a constant temperature incubator at 37 °C. The stability of BM-nano under these two conditions was evaluated by detecting the changes of its particle size and PDI at 0–7 days using DLS. As shown in Figure 3d and 3e, BM-nano exhibited good stability in both PBS and FBS solutions with little change in particle size and PDI over a period of 7 days.

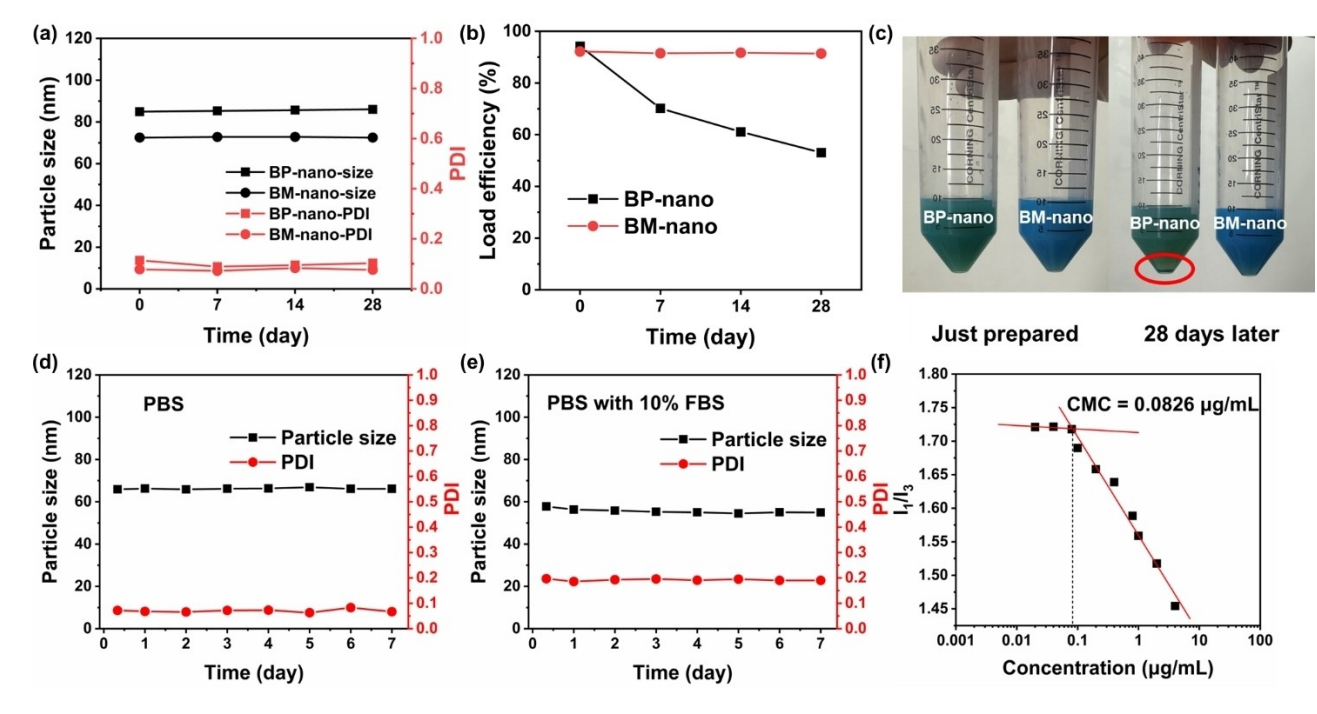


Figure 3. Change of particle size (a) and loading efficiency (b) of BP-nano and BM-nano at room temperature over time. Photograph of BP-nano and BM-nano aqueous solution at room temperature over time. Changes of the particle size and PDI of BM-nano in PBS solution (d) and PBS solution with 10% FBS (e) at 37% over time. Curve of I_1/I_3 as a function of polymer concentrations of BM-nano (f).

5213773, 2024, 20, Downloaded from https://onlinelibtary.wiley.com/doi/10.1002/anie.020402747 by Carnegie Mellon University, Wiley Online Library on [1/4/03/2025]. See the Terms and Conditions (https://onlinelibrary.wiley.com/terms-and-conditions) on Wiley Online Library for rules of use; OA articles are governed by the applicable Creative Commons License and Conditions (https://onlinelibrary.wiley.com/terms-and-conditions) on Wiley Online Library for rules of use; OA articles are governed by the applicable Creative Commons License and Conditions (https://onlinelibrary.wiley.com/terms-and-conditions) on Wiley Online Library for rules of use; OA articles are governed by the applicable Creative Commons License and Conditions (https://onlinelibrary.wiley.com/terms-and-conditions) on Wiley Online Library for rules of use; OA articles are governed by the applicable Creative Commons License and Conditions (https://onlinelibrary.wiley.com/terms-and-conditions) on Wiley Online Library for rules of use; OA articles are governed by the applicable Creative Commons License and Conditions (https://onlinelibrary.wiley.com/terms-and-conditions) on Wiley Online Library for rules of use; OA articles are governed by the applicable Creative Commons License and Conditions (https://onlinelibrary.wiley.com/terms-and-conditions) on Wiley Online Library for rules of use and the use of use and use an

Angewandte
International Edition Chemie

Critical micelle concentration (CMC) is crucial for nanodrugs to maintain structure of nanoparticles after injection into the body during blood circulation. The CMC of BMnano was determined by pyrene fluorescence probe method, based on the intensity ratio at 373 and 384 nm (I_1/I_3) in the pyrene emission spectra (Figure 3d), a low level of CMC value of BM-nano was calculated to be 0.0826 µg/mL, meaning that the disassembly of the nanodrug would only happen when the concentration of PEG-b-PMMA was diluted to this low value, which is beneficial to the maintenance of structure in vivo. Based on the above results, it could be concluded that BM-nano can maintain robust stability during blood circulation before reaching tumor

sites. In summary, BM-nano exhibits excellent stability under physiological conditions, which facilitates its long-term storage, as well as biological applications.

In Vitro Cytotoxicity and Cellular Uptake of BM-nano

The in vitro cytotoxicity of BM-nano against MDA-MB-231, HuH-7, HT-1080 and HCT-116 cells was evaluated using the CCK-8 assay. As shown in Figure 4a–d, the IC $_{50}$ values of BM-nano against the four tumor cells are 1.87 μ M, 2.25 μ M, 7.50 μ M and 3.06 μ M respectively, which maintained potent antitumor activity compared with Cu(BMMODA)Cl $_2$. The

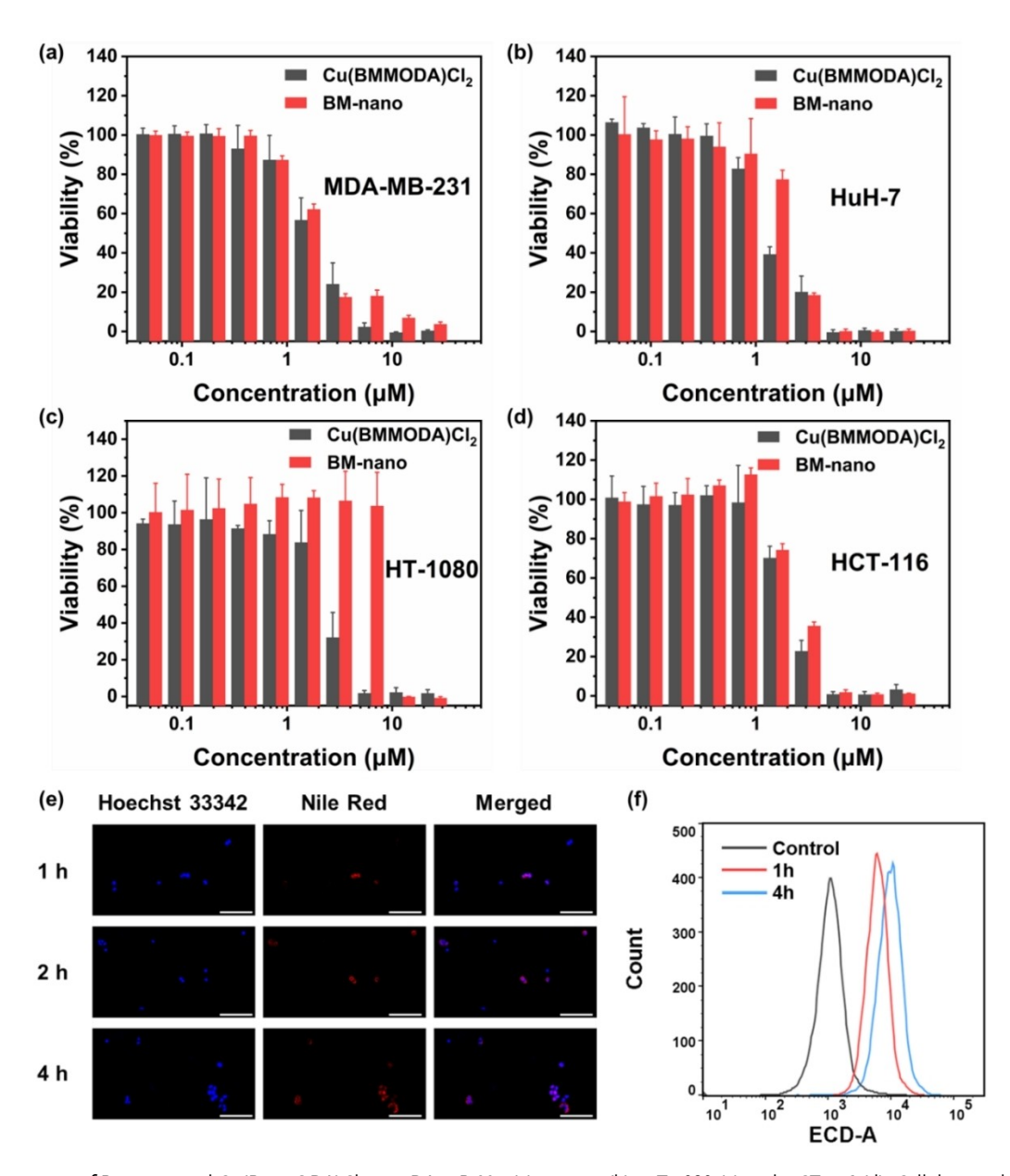
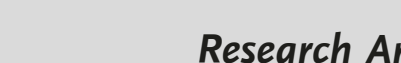


Figure 4. Cytotoxicity of BM-nano and Cu(BMMODA)Cl₂ to MDA-MB-231 (a), HuH-7 (b), HT-1080 (c) and HCT-116 (d), Cellular uptake of BM-nano by MDA-MB-231 cells using CLSM to observe at different time intervals (e). Flow cytometry histogram profiles of MDA-MB-231 cells incubated with BM-nano at different time intervals (f). The untreated cells are used as a control. The scale bar represents 100 μm. Data are represented by mean \pm SD, n=3.

Angewandte



results indicate that the in situ loading of the antitumor copper complex in nanodrug did not significantly affect its antitumor activity. To evaluate the in vitro cellular uptake behavior of BM-nano, nile red (NR) was chosen as the hydrophobic fluorescent probe, which was loaded in BMnano by dissolving NR in MMA before miniemulsion polymerization. Confocal laser scanning microscopy (CLSM) and flow cytometry were used to observe the cellular uptake behavior in MDA-MB-231 cells. As shown in Figure 4e, the MDA-MB-231 cells were incubated with NR-loaded BM-nano for 1 h, 2 h, and 4 h, which were stained with Hoechst 33342. Red fluorescence was observed around or inside the nucleus of cells for 1 h, and the red fluorescence intensity gradually enhanced with the extension of incubation time, indicating that NR-loaded BM-nano could be effectively phagocytosed by cells over time. The slight increase in the intensity of red fluorescence was due to the anticancer copper complex being loaded in situ in the core of nanodrug, which was delivered into the cell with nanodrug at the same time, effected cancer cells and moderated the further phagocytosis. In addition, the results measured by flow cytometry (Figure 4f) were consistent with the results observed by confocal laser scanning microscopy, which further demonstrated the internalization of BM-nano by cancer cells.

Pharmacokinetics and Biodistribution Studies

Nanoparticles with particle size of 20-200 nm have longer circulation time in vivo and tend to accumulate at tumor site compared with small molecular drugs. [29] Pharmacokinetic study of BM-nano was carried out to analyze the retention of BM-nano during blood circulation. The mice experiments were approved by the Ethics Committee of Zhejiang University and conducted in accordance with the guidelines. The pharmacokinetic profiles were obtained by tail vein injection of the same dose (in terms of copper element) of copper Cu(BMMODA)Cl₂ or nanodrug in Sprague-Dawley (SD) rats. The blood was withdrawn at the designed time points, detected by ICP-OES for the plasma concentration of copper element. As displayed in Figure 5a, BM-nano showed a longer circulation time than free Cu-(BMMODA)Cl₂ during 24 h. The copper content in the plasma of rats was 2.86 µg/mL after the injection of BMnano for 24 h, which was 81 % higher than that of the free Cu(BMMODA)Cl₂. Furthermore, we calculated the pharmacokinetic parameters using a noncompartmental model to quantitatively reveal the difference (Table S2). The halflife $(t_{1/2})$ of BM-nano was 47.60 h, which was much longer than that of Cu(BMMODA)Cl₂ (28.55 h), resulting in high plasma concentration of copper after 24 h. BM-nano also shows good stability with the area under the total pharmaco-

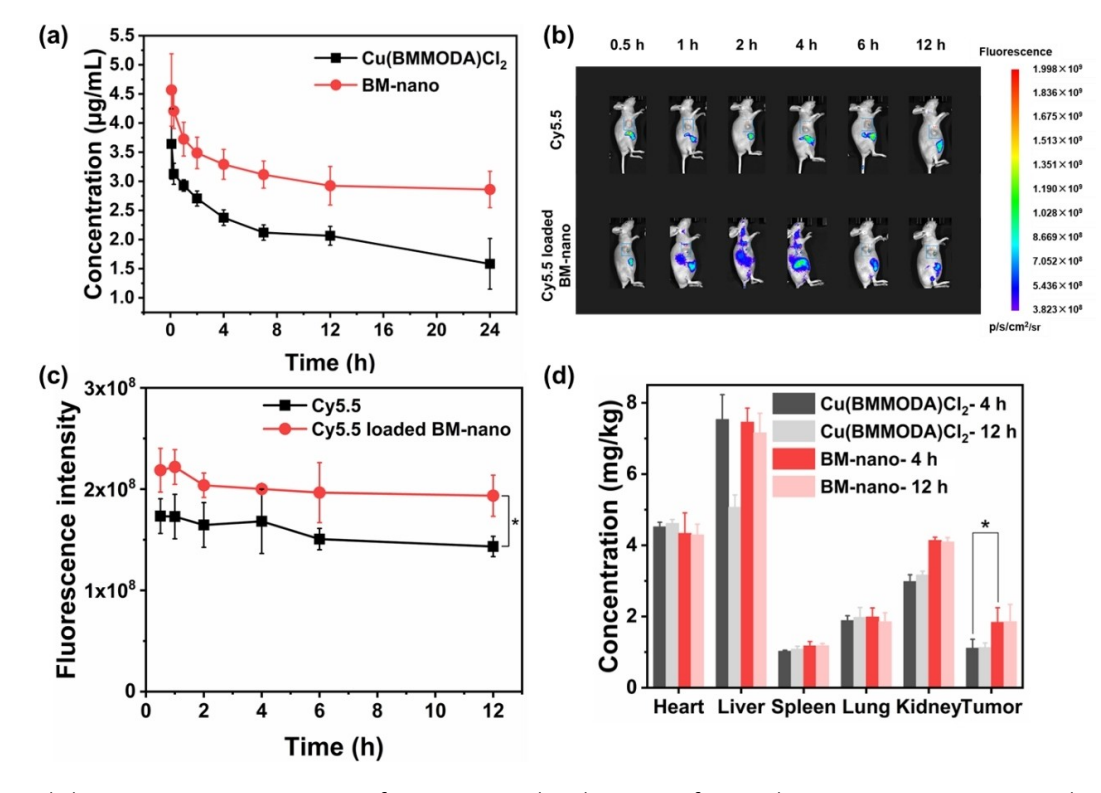


Figure 5. Typical plasma concentration-time curves of Cu(BMMODA)Cl₂ and BM-nano after i.v. administration into SD rats (5 mg/kg) (a). In vivo noninvasive fluorescence images of MDA-MB-231 tumor-bearing nude mice at preset intervals after i.v. administration of free Cy5.5 and Cy5.5loaded BM-nano (b). Fluorescence intensity of MDA-MB-231 tumor-bearing nude mice at tumor site after i.v. administration of free Cy5.5 and Cy5.5-loaded BM-nano (c). Tissue distribution after i.v. administration of Cu(BMMODA)Cl₂ and BM-nano in MDA-MB-231 tumor-bearing nude mice at organs (heart, liver, spleen, lung, and kidney) and tumor (d). Data are represented by mean \pm SD, n=5, significance test was conducted by two-tailed Student's t-test, *: p < 0.05.

5213773, 2024, 20, Downloaded from https://onlinelibtary.wiley.com/doi/10.1002/anie.020402747 by Carnegie Mellon University, Wiley Online Library on [1/4/03/2025]. See the Terms and Conditions (https://onlinelibrary.wiley.com/terms-and-conditions) on Wiley Online Library for rules of use; OA articles are governed by the applicable Creative Commons License and Conditions (https://onlinelibrary.wiley.com/terms-and-conditions) on Wiley Online Library for rules of use; OA articles are governed by the applicable Creative Commons License and Conditions (https://onlinelibrary.wiley.com/terms-and-conditions) on Wiley Online Library for rules of use; OA articles are governed by the applicable Creative Commons License and Conditions (https://onlinelibrary.wiley.com/terms-and-conditions) on Wiley Online Library for rules of use; OA articles are governed by the applicable Creative Commons License and Conditions (https://onlinelibrary.wiley.com/terms-and-conditions) on Wiley Online Library for rules of use; OA articles are governed by the applicable Creative Commons License and Conditions (https://onlinelibrary.wiley.com/terms-and-conditions) on Wiley Online Library for rules of use; OA articles are governed by the applicable Creative Commons License and Conditions (https://onlinelibrary.wiley.com/terms-and-conditions) on Wiley Online Library for rules of use and the use of use and use an

kinetic curve $(AUC_{0\rightarrow\infty})$ of 242.14 µg·h/mL larger than that of Cu(BMMODA)Cl₂ (114.86 μg·h/mL), which derives from the longer mean residence time (MRT $_{0\rightarrow\infty}$, 78.67 h) and lower rate of total body clearance (Cl_t, 1.98 mL/h/kg) of BM-nano than the corresponding parameters of Cu-(BMMODA)Cl₂ (41.76 h and 4.18 mL/h/kg) respectively. In addition, the low apparent volume of distribution of BMnano (V_d, 136.15 mL/kg) revealed that BM-nano can decrease the rate of excretion in blood more efficiently compared with Cu(BMMODA)Cl₂ (172.17 mL/kg). The results prove that BM-nano possesses lower blood clearance rate and longer circulation time than Cu(BMMODA)Cl₂ in the blood.

To further validate the retention of BM-nano at tumor site, Cy5.5-loaded BM-nano solution was prepared by dissolving Cy5.5 in MMA before miniemulsion polymerization, which was injected into tumor-bearing nude mice by tail vein injection. Free Cy5.5 was also injected for a comparison. Real-time fluorescence imaging was recorded during the experimental period of 12 h (Figure 5b) to detect the distribution of BM-nano in nude mice. Within 12 hours, the fluorescence intensity of free Cy5.5 in vivo was significantly weaker than that of BM-nano loaded with Cy5.5, indicating that free Cy5.5 was rapidly cleared during blood circulation, resulting in short retention time, and the loading by nanoparticles was able to slow down this process and prolong the retention time of Cy5.5 in blood. This result can be ascribed to the low molecular weight of Cy5.5, which made easier clearance. At tumor site, the fluorescence intensity of free Cy5.5 remained weak during the whole observation period while the fluorescence intensity of Cy5.5loaded BM-nano was high around 12 h post injection. Figure 5c quantitatively demonstrates the difference in fluorescence intensity between free Cy5.5 and Cy5.5-loaded BM-nano at the tumor site. The fluorescence intensity at tumor site with Cy5.5-loaded BM-nano treated was 35.7 % higher than that of free Cy5.5. These results further confirm that BM-nano can prolong the retention time in the blood and accumulate at the tumor site.

Aside from the plasma pharmacokinetics, the biodistribution was investigated in major organs (heart, liver, spleen, lungs, and kidneys) and tumor sites. The nude mice were analyzed at 4 h and 12 h after the injection of Cu-(BMMODA)Cl₂ or nanodrug BM-nano into the tail vein of tumor-bearing nude mice, and the content of copper in the biodistribution profiles (Figure 5d) showed that there was no significant difference in the concentration of copper in heart, spleen and lungs for the mice injected with the nanodrug and free Cu(BMMODA)Cl₂ at 4 and 12 h. However, the concentrations in liver and kidney of mice administered with BM-nano were higher than those receiving the Cu(BMMODA)Cl₂. This result indicates that compared with the free Cu(BMMODA)Cl2, BM-nano promoted the accumulation of copper in vivo and slowing down the excretion of copper through the liver, showing the effect of prolonging the circulation time. In addition, the copper content in tumor tissues was 1.86 mg/kg after the injecting of BM-nano for 12 h, which was 64.6 % higher than the 1.13 mg/kg of Cu(BMMODA)Cl₂, further demonstrating

that BM-nano effectively promoted drug retention at tumor tissues.

In Vivo Antitumor Activity

In vivo antitumor activity of BM-nano was further evaluated based on its promising in vitro antitumor activity with MDA-MB-231 tumor-bearing nude mice. (BMMODA)Cl2 and BM-nano were injected by tail vein at a dose of 1 mg (Cu)/kg every 2 days, as well as PBS and cisplatin(1 mg (Pt)/kg). As shown in Figure 6a, the tumor growth in the mice treated with Cu(BMMODA)Cl₂ and BM-nano were remarkably suppressed compared to PBStreated group. The relative tumor sizes of the PBS groups increased by 789%, which were 1.8-fold and 63-fold higher than those of the Cu(BMMODA)Cl2 and BM-nano group after 14 days. In addition, Cu(BMMODA)Cl₂ and BM-nano showed superior antitumor activity to cisplatin at the same dose of 1 mg (metal)/kg with the tumor sizes were 69.1 % and 14.4% of cisplatin group after 14 days, while more than 3.25 mg (metal)/kg of cisplatin injection dose was required to produce good inhibitory effect on MDA-MB-231 tumors in vivo in general, [30] which was consistent with the above in vitro cytotoxicity results. The results showed that Cu-(BMMODA)Cl₂ had a good in vivo antitumor activity superior to that of cisplatin at a low drug dose, and the copper-containing nanodrug BM-nano loaded with the same dose of Cu(BMMODA)Cl2 could further improve its in vivo antitumor activity potently, which attributed to the fact that BM-nano could prolong the drug retention time, and be efficiently ingested by the tumor cells and selective retention at the tumor site. In addition, as shown in Figure 6b, the body weight of mice in all groups increased slowly at the drug dose of 1 mg/kg, which indicated that BM-nano could produce excellent tumor inhibition at a drug dose that did not produce obvious toxic side effects in mice. This phenomenon was not only led by the specially targeting ability of BM-nano towards tumor tissue, but also arose from the elevated toxicity of copper complexes exhibited on cancer cells in contrast to normal cells.[31] The elevated toxicity was due to the upregulation of the copper transporter CTR1 resulting from the high oxygen consumption in cancer cells, leading to the increase of intracellular copper compared with normal cells.[32] Therefore, the intracellular copper concentration in cancer is more likely to exceed the cell-death induction threshold concentration.^[33] Besides, in the acidic environment on tumor tissue, [34] the hetero-atom (such as the nitrogen atom) on the ligand could be protonated, so that the copper ions were easier to release in the tumor cells.^[35] The tumor suppressive effect was further confirmed by tumor weight and photographs of tumors isolated from tumor-bearing nude mice (Figure 6c and 6d). The tumor inhibition rates of the Cu(BMMODA)Cl₂ and the BM-nano were 37.2% and 90.0% respectively, which were superior to the 22.8 % of cisplatin.

The tumors in each group were taken out for histopathology and immunofluorescence analysis at the end of treatment to further evaluate the tumor suppression after

Research Articles

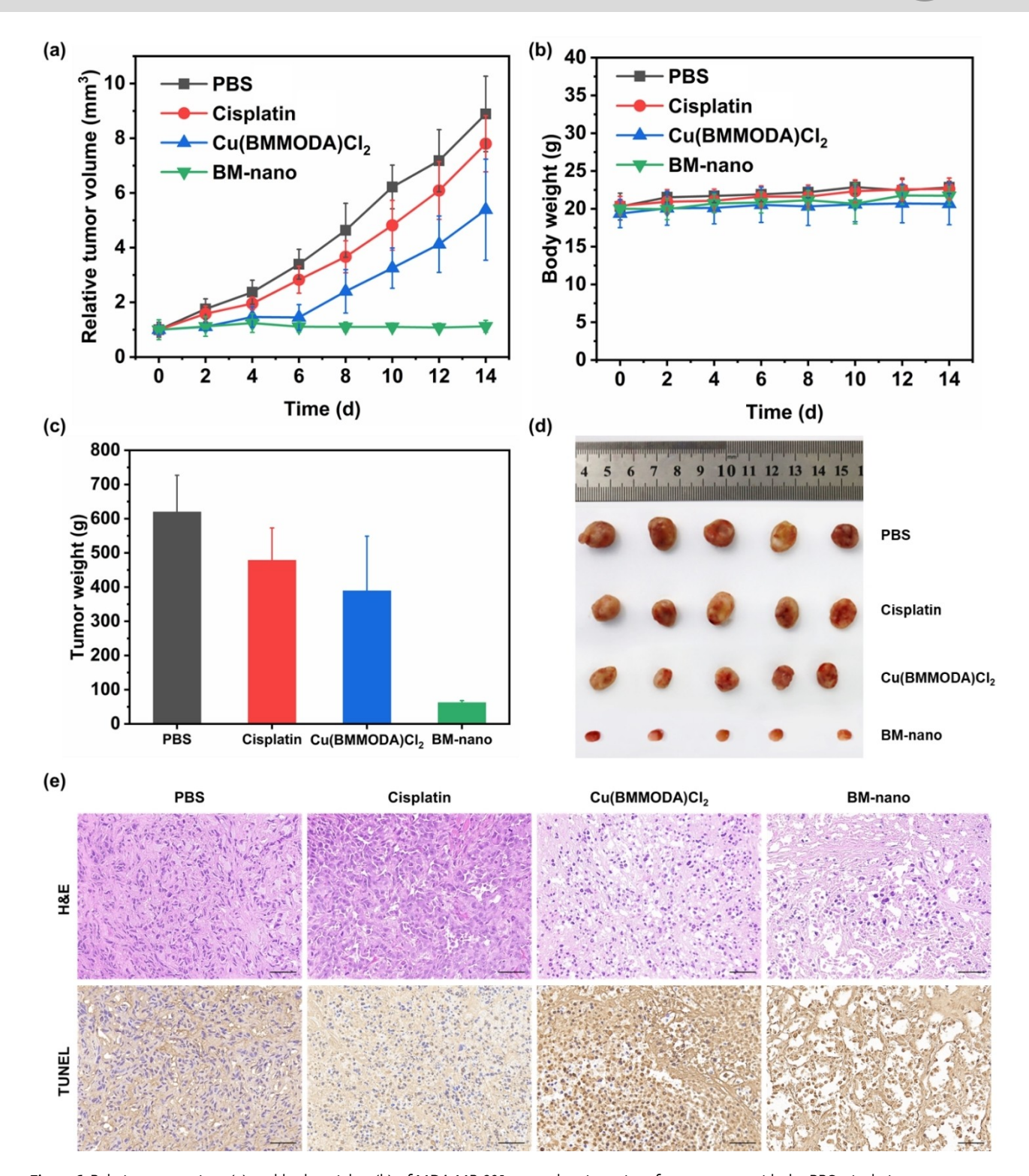


Figure 6. Relative tumor sizes (a) and body weights (b) of MDA-MB-231 tumor-bearing mice after treatment with the PBS, cisplatin, $Cu(BMMODA)Cl_2$ and BM-nano every 2 days, respectively. Tumor weights (c) and photograph (d) of MDA-MB-231 tumor-bearing mice after treatment with the PBS, cisplatin, $Cu(BMMODA)Cl_2$ and BM-nano isolated at day 14. H&E and TUNEL staining of tumors excised from the mice at day 14. The scale bar represents 50 μ m (e). Data are represented by mean \pm SD, n = 5.

treatment with different drugs. As shown in Figure 6e, for hematoxylin and eosin (H&E) images, the tumor cells were dense in PBS group with large and deeply stained nuclei, presenting rapid tumor proliferation. Conversely, in Cu-

(BMMODA)Cl₂ and BM-nano groups, cell density was significantly reduced, nuclei were collapsed and nuclear fragments could be observed. In addition, cells in the BM-nano group showed extensive necrosis, indicating the most

15213773, 2024, 20, Downloaded from https://onlinelibrary.wiley.com/doi/10.1002/anie.202402747 by Carengie Mellon University, Wiley Online Library on [14/03/2025]. See the Terms and Conditions (https://onlinelibrary.wiley.com/terms-and-conditions) on Wiley Online Library for rules of use; OA articles are governed by the applicable Creative Commons Licensean Conditions (https://onlinelibrary.wiley.com/terms-and-conditions) on Wiley Online Library for rules of use; OA articles are governed by the applicable Creative Commons Licensean Conditions (https://onlinelibrary.wiley.com/terms-and-conditions) on Wiley Online Library for rules of use; OA articles are governed by the applicable Creative Commons Licensean Conditions (https://onlinelibrary.wiley.com/terms-and-conditions) on Wiley Online Library for rules of use; OA articles are governed by the applicable Creative Commons Licensean Conditions (https://onlinelibrary.wiley.com/terms-and-conditions) on Wiley Online Library for rules of use; OA articles are governed by the applicable Creative Commons Licensean Conditions (https://onlinelibrary.wiley.com/terms-and-conditions) on Wiley Online Library for rules of use; OA articles are governed by the applicable Creative Commons Licensean Conditions (https://onlinelibrary.wiley.com/terms-and-conditions) on Wiley Online Library for rules of use; OA articles are governed by the applicable Creative Commons (https://onlinelibrary.wiley.com/terms-and-conditions) on the applicable Creative Common



significant tumor inhibition. For terminal transferase-mediated dUTP nick end-labeling (TUNEL), the nuclear staining degree of BM-nano group was significantly higher than that of cisplatin group, implying that BM-nano had the strongest ability to induce apoptosis of tumor cells and showed significant tumor treatment effects among all the groups, which further supported the results from H&E images.

Conclusion

In this study, copper-containing nanoparticles with uniform spheric morphology were directly prepared via miniemulsion AGET ATRP using Cu(BMMODA)Cl₂ as catalyst, which was in situ incorporated in the nanoparticles as a antitumor agent. The resulting aqueous dispersion of copper-containing nanoparticles was directly used as copper nanodrug for anticancer chemotherapy with the high copper loading efficiency. Furthermore, the nanodrug formulation not only increased the blood circulation time, decreased the total body clearance, enhanced the accumulation at tumor sites compared with free copper complex, but also further exhibited more potent antitumor activity in vitro and vivo than cisplatin. This work provides a novel strategy for precise and large-scale preparation of copper nanodrugs with simplified synthetic procedures and raw materials, which is expected to facilitate their clinical applications.

Supporting Information

The authors have cited additional references within the Supporting Information. [19e,28, 36]

Acknowledgements

This work was supported by the National Key Research and Development Program of China (2019YFE0117500), Shan-xi-Zheda Institute of Advanced Materials and Chemical Engineering (2022SZ-AT001), the National Natural Science Foundation of China (22275164 and 22071216) and US NSF (DMR 2202747).

Conflict of Interest

The authors declare no conflict of interest.

Data Availability Statement

The data that support the findings of this study are available from the corresponding author upon reasonable request.

Keywords: atom transfer radical polymerization \cdot miniemulsion polymerization \cdot nanodrugs \cdot copper complex \cdot anti-tumor

- a) F. Arnesano, G. Natile, Coord. Chem. Rev. 2009, 253, 2070– 2081; b) A. M. P. Romani, Biochem. Pharmacol. 2022, 206, 115323.
- [2] Y. Jung, S. J. Lippard, Chem. Rev. 2007, 107, 1387–1407.
- [3] E. J. Ge, A. I. Bush, A. Casini, P. A. Cobine, J. R. Cross, G. M. DeNicola, Q. P. Dou, K. J. Franz, V. M. Gohil, S. Gupta, S. G. Kaler, S. Lutsenko, V. Mittal, M. J. Petris, R. Polishchuk, M. Ralle, M. L. Schilsky, N. K. Tonks, L. T. Vahdat, L. Van Aelst, D. Xi, P. Yuan, D. C. Brady, C. J. Chang, *Nat. Rev. Cancer* 2022, 22, 102–113.
- [4] a) M. O'Connor, A. Kellett, M. McCann, G. Rosair, M. McNamara, O. Howe, B. S. Creaven, S. n. McClean, A. Foltyn-Arfa Kia, D. O'Shea, J. Med. Chem. 2012, 55, 1957–1968;
 b) B. B. Hasinoff, X. Wu, A. A. Yadav, D. Patel, H. Zhang, D.-S. Wang, Z.-S. Chen, J. C. Yalowich, Biochem. Pharmacol. 2015, 93, 266–276;
 c) D. Mahendiran, S. Amuthakala, N. S. Bhuvanesh, R. S. Kumar, A. K. Rahiman, RSC Adv. 2018, 8, 16973–16990.
- [5] a) C. Slator, N. Barron, O. Howe, A. Kellett, ACS Chem. Biol. 2016, 11, 159–171; b) J. Shao, M. Li, Z. Guo, C. Jin, F. Zhang, C. Ou, Y. Xie, S. Tan, Z. Wang, S. Zheng, Cell Commun. Signaling 2019, 17, 1–18; c) K. Jomova, L. Hudecova, P. Lauro, M. Simunková, Z. Barbierikova, M. Malcek, S. H. Alwasel, I. M. Alhazza, C. J. Rhodes, M. Valko, J. Inorg. Biochem. 2022, 226, 111635.
- [6] a) S. T. Chew, K. M. Lo, S. K. Lee, M. P. Heng, W. Y. Teoh, K. S. Sim, K. W. Tan, Eur. J. Med. Chem. 2014, 76, 397–407; b) J. D. Conner, W. Medawala, M. T. Stephens, W. H. Morris, J. E. Deweese, P. L. Kent, J. J. Rice, X. Jiang, E. C. Lisic, Open J. Inorg. Chem. 2016, 6, 146–154; c) S. Sandhaus, R. Taylor, T. Edwards, A. Huddleston, Y. Wooten, R. Venkatraman, R. T. Weber, A. González-Sarrías, P. M. Martin, P. Cagle, Y.-C. Tse-Dinh, S. J. Beebe, N. Seeram, A. A. Holder, Inorg. Chem. Commun. 2016, 64, 45–49.
- [7] a) K. G. Daniel, D. Chen, S. Orlu, Q. C. Cui, F. R. Miller, Q. P. Dou, *Breast Cancer Res.* 2005, 7, 897–908; b) X. Chen, X. Zhang, J. Chen, Q. Yang, L. Yang, D. Xu, P. Zhang, X. Wang, J. Liu, *Eur. J. Pharmacol.* 2017, 815, 147–155.
- [8] P. Tsvetkov, S. Coy, B. Petrova, M. Dreishpoon, A. Verma, M. Abdusamad, J. Rossen, L. Joesch-Cohen, R. Humeidi, R. D. Spangler, J. K. Eaton, E. Frenkel, M. Kocak, S. M. Corsello, S. Lutsenko, N. Kanarek, S. Santagata, T. R. Golub, *Science* 2022, 375, 1254–1261.
- [9] K. Cho, X. Wang, S. Nie, Z. Chen, D. M. Shin, Clin. Cancer Res. 2008, 14, 1310–1316.
- [10] a) K. Nurgali, R. T. Jagoe, R. Abalo, Front. Pharmacol. 2018,
 9, 245; b) H. Was, A. Borkowska, A. Bagues, L. Tu, J. Y. Liu,
 Z. Lu, J. A. Rudd, K. Nurgali, R. Abalo, Front. Pharmacol. 2022, 13, 750507.
- [11] a) L. E. Gerlowski, R. K. Jain, Microvasc. Res. 1986, 31, 288–305; b) Y. Matsumura, H. Maeda, Cancer Res. 1986, 46, 6387–6392; c) H. Maeda, Adv. Drug Delivery Rev. 2015, 91, 3–6; d) J. Fang, W. Islam, H. Maeda, Adv. Drug Delivery Rev. 2020, 157, 142–160; e) H. Chu, R. Sun, J. Sheng, X. Li, X. Li, W. Wang, L. Teng, W. Zhu, React. Funct. Polym. 2023, 191, 105654.
- [12] a) J. D. Byrne, T. Betancourt, L. Brannon-Peppas, Adv. Drug Delivery Rev. 2008, 60, 1615–1626; b) A. Alibakhshi, F. A. Kahaki, S. Ahangarzadeh, H. Yaghoobi, F. Yarian, R. Arezumand, J. Ranjbari, A. Mokhtarzadeh, M. de la Guardia, J. Controlled Release 2017, 268, 323–334; c) C. Chen, T. Ma, W. Tang, X. Wang, Y. Wang, J. Zhuang, Y. Zhu, P. Wang, Nanoscale Horiz. 2020, 5, 986–998; d) M. Landgraf, C. A. Lahr, I. Kaur, A. Shafiee, A. Sanchez-Herrero, P. W. Janowicz, A. Ravichandran, C. B. Howard, A. Cifuentes-Rius, J. A. McGovern, Biomaterials 2020, 240, 119791.





- [13] a) K. D. Patel, L. Barrios Silva, Y. Park, T. Shakouri, Z. Keskin-Erdogan, P. Sawadkar, K. J. Cho, J. C. Knowles, D. Y. S. Chau, H. W. Kim, *Mater. Today Nano* 2022, 18; b) J. Shi, P. W. Kantoff, R. Wooster, O. C. Farokhzad, *Nat. Rev. Cancer* 2017, 17, 20–37.
- [14] a) I. de Lázaro, D. J. Mooney, Nat. Mater. 2021, 20, 1469–1479;
 b) S. Wang, K. Cheng, K. Chen, C. Xu, P. Ma, G. Dang, Y. Yang, Q. Lei, H. Huang, Y. Yu, Y. Fang, Q. Tang, N. Jiang, H. Miao, F. Liu, X. Zhao, N. Li, Nano Today 2022, 45, 101512.
- [15] a) J. Guo, X. Gao, L. Su, H. Xia, G. Gu, Z. Pang, X. Jiang, L. Yao, J. Chen, H. Chen, Biomaterials 2011, 32, 8010–8020; b) T. Thambi, V. G. Deepagan, H. Y. Yoon, H. S. Han, S.-H. Kim, S. Son, D.-G. Jo, C.-H. Ahn, Y. D. Suh, K. Kim, I. Chan Kwon, D. S. Lee, J. H. Park, Biomaterials 2014, 35, 1735–1743; c) D. Hu, L. Chen, Y. Qu, J. Peng, B. Chu, K. Shi, Y. Hao, L. Zhong, M. Wang, Z. Qian, Theranostics 2018, 8, 1558; d) J. D. Yuan, D. L. ZhuGe, M. Q. Tong, M. T. Lin, X. F. Xu, X. Tang, Y. Z. Zhao, H. L. Xu, Artif. Cells, Nanomed., Biotechnol. 2018, 46, 302–313; e) Q. Cai, J. Jiang, H. Zhang, P. Ge, L. Yang, W. Zhu, ACS Appl. Mater. Interfaces 2021, 13, 19387–19397.
- [16] a) J. K. Oh, R. Drumright, D. J. Siegwart, K. Matyjaszewski, Prog. Polym. Sci. 2008, 33, 448-477; b) K. Matyjaszewski, Adv. Mater. 2018, 30, e1706441; c) N. Corrigan, K. Jung, G. Moad, C. J. Hawker, K. Matyjaszewski, C. Boyer, Prog. Polym. Sci. 2020, 111, 101311; d) K. Matyjaszewski, N. V. Tsarevsky, J. Am. Chem. Soc. 2014, 136, 6513-6533; e) K. Matyjaszewski, N. V. Tsarevsky, Nat. Chem. 2009, 1, 276-288; f) J. F. Lutz, J. M. Lehn, E. W. Meijer, K. Matyjaszewski, Nat. Rev. Mater. 2016, 1, 16024; g) K. Matyjaszewski, W. Jakubowski, K. Min, W. Tang, J. Y. Huang, W. A. Braunecker, N. V. Tsarevsky, Proc. Natl. Acad. Sci. USA 2006, 103, 15309-15314; h) T. E. Patten, J. H. Xia, T. Abernathy, K. Matyjaszewski, Science 1996, 272, 866-868; i) N. V. Tsarevsky, K. Matyjaszewski, Chem. Rev. 2007, 107, 2270-2299; j) K. Matyjaszewski, J. H. Xia, Chem. Rev. 2001, 101, 2921-2990; k) J. S. Wang, K. Matyjaszewski, J. Am. Chem. Soc. 1995, 117, 5614-5615.
- [17] a) W. Tang, K. Matyjaszewski, Macromolecules 2006, 39, 4953–4959; b) F. Lorandi, K. Matyjaszewski, Isr. J. Chem. 2019, 60, 108–123; c) F. Lorandi, M. Fantin, A. A. Isse, A. Gennaro, K. Matyjaszewski, Electrochim. Acta 2018, 260, 648–655; d) T. G. Ribelli, F. Lorandi, M. Fantin, K. Matyjaszewski, Macromol. Rapid Commun. 2019, 40, e1800616; e) W. Tang, Y. Kwak, W. Braunecker, N. V. Tsarevsky, M. L. Coote, K. Matyjaszewski, J. Am. Chem. Soc. 2008, 130, 10702–10713; f) N. V. Tsarevsky, W. A. Braunecker, K. Matyjaszewski, J. Organomet. Chem. 2007, 692, 3212–3222.
- [18] a) V. Oliveri, Coord. Chem. Rev. 2020, 422, 213474; b) Y. Ji, F. Dai, B. Zhou, Free Radical Biol. Med. 2018, 129, 215–226; c) S. Tardito, I. Bassanetti, C. Bignardi, L. Elviri, M. Tegoni, C. Mucchino, O. Bussolati, R. Franchi Gazzola, L. Marchiò, J. Am. Chem. Soc. 2011, 133, 6235–6242; d) C. Santini, M. Pellei, V. Gandin, M. Porchia, F. Tisato, C. Marzano, Chem. Rev. 2014, 114, 815–862.
- [19] a) G. Szczepaniak, L. Fu, H. Jafari, K. Kapil, K. Matyjaszewski, Acc. Chem. Res. 2021, 54, 1779–1790; b) W. W. Li, K. Min, K. Matyjaszewski, F. Stoffelbach, B. Charleux, Macromolecules 2008, 41, 6387–6392; c) F. Stoffelbach, B. Belardi, J. M. R. C. A. Santos, L. Tessier, K. Matyjaszewski, B. Charleux, Macromolecules 2007, 40, 8813–8816; d) W. Zhu, M. Zhong, W. Li, H. Dong, K. Matyjaszewski, Macromolecules

- **2011**, *44*, 1920–1926; e) A. M. Elsen, J. Burdyńska, S. Park, K. Matyjaszewski, *Macromolecules* **2012**, *45*, 7356–7363.
- [20] B. L. Banik, P. Fattahi, J. L. Brown, Wiley Interdiscip. Rev. Nanomed. Nanobiotechnol. 2016, 8, 271–299.
- [21] Q. Wen, Q. Q. Cai, P. Fu, D. Chang, X. Y. Xu, T. J. Wen, G. P. Wu, W. P. Zhu, L. S. Wan, C. J. Zhang, X. H. Zhang, Q. Jin, Z. L. Wu, C. Gao, H. K. Zhang, N. Huang, C. Z. Li, H. Y. Li, Chin. Chem. Lett. 2023, 34, 107592.
- [22] N. Bortolamei, A. A. Isse, V. B. Di Marco, A. Gennaro, K. Matyjaszewski, *Macromolecules* 2010, 43, 9257–9267.
- [23] a) R. Sun, Q. Luo, X. Li, X. Huang, L. Teng, Z. Shen, W. Zhu, Mater. Today Nano 2021, 14, 100115; b) W. Zhu, Y. Wang, Q. Zhang, Z. Shen, J. Polym. Sci. Part A 2011, 49, 4886-4893; c) Y. Wang, Q. J. Luo, L. L. Gao, C. Gao, H. Du, G. Y. Zha, X. D. Li, Z. Q. Shen, W. P. Zhu, Biomater. Sci. 2014, 2, 1367–1376; d) W. Song, M. Das, Y. Xu, X. Si, Y. Zhang, Z. Tang, X. Chen, Mater. Today Nano 2019, 5, 100029.
- [24] K. Ute, N. Miyatake, K. Hatada, *Polymer* **1995**, *36*, 1415–1419.
- [25] M. H. Gutierrez, Villarreal, J. Rodríguez, Velazquez, J. Appl. Polym. Sci. 2007, 105, 2370–2375.
- [26] F. J. Schork, Y. Luo, W. Smulders, J. P. Russum, A. Butté, K. Fontenot, in *Polymer Particles* (Ed.: M. Okubo), Springer Berlin Heidelberg, Berlin, Heidelberg, 2005, 129–255.
- [27] S. Soares, J. Sousa, A. Pais, C. Vitorino, *Front. Chem.* **2018**, *6*, 360
- [28] G. Basu Ray, I. Chakraborty, S. P. Moulik, J. Colloid Interface Sci. 2006, 294, 248–254.
- [29] M. Elsabahy, K. L. Wooley, Chem. Soc. Rev. 2012, 41, 2545– 2561
- [30] Q. Cao, D. J. Zhou, Z. Y. Pan, G. G. Yang, H. Zhang, L. N. Ji, Z. W. Mao, Angew. Chem. Int. Ed. 2020, 132, 18715–18721.
- [31] a) F. Mohammadizadeh, S. K. Falahati-Pour, A. Rezaei, M. Mohamadi, M. R. Hajizadeh, M. R. Mirzaei, A. Khoshdel, M. A. Fahmidehkar, M. Mahmoodi, *BioMetals* 2018, 31, 233–242; b) R. D. Bao, X. Q. Song, Y. J. Kong, F. F. Li, W. H. Liao, J. Zhou, J. H. Zhang, Q. H. Zhao, J. Y. Xu, C. S. Chen, M. J. Xie, *J. Inorg. Biochem.* 2020, 208, 111103.
- [32] L. M. Ruiz, A. Libedinsky, A. A. Elorza, Front. Mol. Biosci. 2021, 8, 711227.
- [33] A. Gupte, R. J. Mumper, Cancer Treat. Rev. 2009, 35, 32-46.
- [34] a) M. Gu, X. Wang, T. B. Toh, E. K. Chow, *Drug Discovery Today* 2018, 23, 1043–1052; b) Y. Kato, S. Ozawa, C. Miyamoto, Y. Maehata, A. Suzuki, T. Maeda, Y. Baba, *Cancer Cell Int.* 2013, 13, 89.
- [35] a) E. C. Ording-Wenker, M. van der Plas, M. A. Siegler, C. Fonseca Guerra, E. Bouwman, *Chem. Eur. J.* 2014, 20, 16913–16921; b) E. J. Ashford, V. Naldi, R. O'Dell, N. C. Billingham, S. P. Armes, *Chem. Commun.* 1999, 1285–1286; c) F. Kou, S. Zhu, H. Lin, W. Chen, Y. Chen, M. Lin, *Polyhedron* 1997, 16, 2021–2028.
- [36] a) K. Jankova, X. Chen, J. Kops, W. Batsberg, Macromolecules 1998, 31, 538–541; b) J. Gabrielsson, D. Weiner, in Computational Toxicology: Volume I (Eds.: B. Reisfeld, A. N. Mayeno), Humana Press, Totowa, NJ, 2012, pp. 377–389.

Manuscript received: February 7, 2024 Accepted manuscript online: March 15, 2024 Version of record online: April 8, 2024